

Defects in swift heavy ion irradiated n-4H-SiC

S.M. Tunhuma*, M. Diale, J.M. Nel, M.J. Madito, T.T. Hlatshwayo, F.D. Auret

Department of Physics, University of Pretoria, Private Bag X20, Pretoria 0002, South Africa



A B S T R A C T

We have used confocal Raman spectroscopy, atomic force microscopy (AFM), Binary collision approximations and Deep level transient spectroscopy (DLTS) to study the defects introduced in n-type 4H-SiC by 167 MeV Xe^{26+} ions (swift heavy ions (SHIs)). Moderately doped epitaxial layers were irradiated with SHIs to a fluence of $5 \times 10^{11} \text{ cm}^{-2}$ at room temperature. Raman spectroscopy was used to investigate the effects of irradiation on the crystal structure. Raman intensity reduced after irradiation but the overall bond structure was conserved. Cluster spectra from confocal Raman spectroscopy showed a damage impact that was consistent with SRIM simulations. AFM showed that the incident radiation resulted in elongated protrusions. The virgin samples contained the $E_{0.09}$, $E_{0.12}$, $E_{0.15}$ and $E_{0.65}$ as the only electrically active defects. After irradiation the $E_{0.40}$ and $E_{0.71}$ defects were introduced.

1. Introduction

Modern day developments in the space, aviation and nuclear energy industry require radiation hard electronic materials. Failure of the Fobos grunt space mission is one example that bears testimony to this assertion. The multi-million dollar space vehicle's demise was attributed to heavy ion irradiation damage on a semiconductor chip which was vital to its electronic functionality [1]. Catastrophic consequences of ion irradiation on devices resulted in monumental loses on the scientific fraternity. There is therefore a need to understand the fundamental physics of radiation damage on electronics so as to develop more tolerant materials.

Silicon carbide (SiC) is one such material that has been shown to be stable under harsh radiation environments [2–5]. The threshold displacement energy of the material is remarkably high with 35 eV in Si and 20 eV in C [6]. These values are almost triple when compared to those of gallium arsenide which is also a radiation hard material [7]. Threshold energy refers to the minimum energy a lattice atom receives before being displaced to an interstitial position in an ion-solid interaction at low temperatures [8]. In-order to apply SiC to radiation-hard devices, an in-depth knowledge of its response in such environments and the defect migration energy therein, is required for refined control purposes. Epitaxial SiC has great potential for high end electronic applications as a substrate for the growth of graphene. For defect engineering on such devices, it is important to have a thorough understanding of the nature and occurrence of irradiation induced defects in the substrate [5].

Several studies have been carried out to create harsh radiation conditions from heavy ions on SiC under controlled environments, and probe the ensuing material perturbations. Sorieul et al. studied heavy

ion irradiated α -SiC using Raman spectroscopy and showed that the structure strongly changes with increasing radiation dose [9]. Kalinina et al. irradiated 4H-SiC UV detectors with 167 MeV Xe ions and showed that the service life and radiation endurance of the devices increased at higher temperatures [10]. In an electrical study, Kalinina et al. also irradiated 4H-SiC with 245 MeV Kr, and showed that it increased the concentration of Z_1 levels but the origin and nature of defects was not discussed [11].

In this study Raman spectroscopy, atomic force microscopy (AFM) and deep level transient spectroscopy (DLTS) were used to study the disorder and electrically active defects induced by 167 MeV Xe^{+26} ion irradiation. The aim was to understand the nature and occurrence of defects formed under swift heavy ion irradiation mainly in the electron energy loss regime. To date, swift heavy ion implantation and amorphization mechanisms in SiC, remain poorly understood [9,12,13]. A comprehensive knowledge on the morphological changes and structural modifications brought in by incident ions irradiation and implantation is critical to understand and implement defect formation in silicon carbide.

2. Experimental details and binary collision approximation (BCA) methodology

Nitrogen doped, n-type (0001) oriented 4H-SiC (8° off axis) wafers supplied by Cree inc were used. The wafers consisted of a $6.0 \mu\text{m}$ epitaxial layer of doping density $6 \times 10^{16} \text{ cm}^{-3}$ grown on a highly doped substrate of approximately 10^{18} cm^{-3} . The samples were cleaned in a two-step procedure that involved degreasing and then wet etching. Degreasing was done by boiling for 5 min each in trichloroethylene, acetone then methanol followed by rinsing in deionised water $18.2 \text{ M}\Omega$.

* Corresponding author.

E-mail address: u13259394@tuks.co.za (S.M. Tunhuma).

cm. Etching was done by dipping the samples in 2% Hydrofluoric acid for 1 min in order to remove the native oxide layer.

Room temperature irradiation of 167 MeV, Xe^{+26} ions was done on the epitaxial layer at a fluence of $5 \times 10^{11} \text{ cm}^{-2}$ at the Joint Institute of Nuclear Research in Dubna, Russia using the IC-100 FLNR cyclotron. Raman spectra were recorded on the epitaxial layer with a T64000 series II triple spectrometer system from HORIBA scientific, Jobin Yvon Technology, using the 514.3 nm laser line of a coherent Innova 70C series Ar⁺ laser (spot size ~ 2 mm) at power of 0.17 mW with a resolution of 2 cm^{-1} . Confocal Raman spectroscopy was carried out using a Witec alpha 300 RAS + Raman spectrometer with the 532 nm laser at a power of 5 mW.

Atomic force microscopy was performed on pristine and irradiated samples using a Bruker Dimension Icon Nanoscope 5 scanning probe microscope with ScanAsyst.

Irradiation was also carried out on the epitaxial layers of samples obtained from the same wafer which had a 3000 Å nickel ohmic contact deposited on the highly doped side of the samples. Ni Schottky contacts where then deposited to form Schottky barrier diodes on the epitaxial layer. DLTS measurements were performed in the 40–370 K temperature range at a quiescent reverse bias of -5 V and a filling pulse of 1 V. The pulse width was 1.0 ms. Arrhenius analysis was done according to the equation [14]

$$e_n = \sigma_n \langle v_{th} \rangle \frac{g_0 N_c}{g_1} \exp\left(-\frac{E_c - E_t}{k_B T}\right) \quad (1)$$

Eq. (1) gives the emission rate as a function of temperature T , where $\langle v_{th} \rangle$ is the thermal velocity of electrons, $(E_c - E_t)$ is the activation energy, N_c is the density of conduction band states, g_0 and g_1 are the degeneracy terms referring to the states before and after electron emission and k_B is the Boltzmann constant.

Mont Carlo simulations of Xe interactions with SiC have been performed in the framework of the binary collision approximation using the SRIM code [15]. using displacement energies of 20 and 35 eV for the C and Si respectively. The ion fluence was converted into displacements per atom (dpa) using the following equation

$$dpa = \frac{\text{vac/ion}^0_A}{\rho_c} \times \phi \quad (2)$$

where ϕ is the ion fluence, ρ_c is the theoretical density of 4H-SiC ($9.641 \times 10^{22} \text{ at/cm}^3$) and vac/ion Å is the vacancy per ion ratio from SRIM.

3. Results and discussion

3.1. Binary collision approximation

Relative density of Xe atoms and the defect distributions as a function of depth are plotted in Fig. 1. Maximum electron energy loss was $20.42 \text{ keV nm}^{-1}$ and the maximum nuclear energy loss was $0.8361 \text{ keV nm}^{-1}$ as shown in Fig. 2. Swift heavy ions do not produce latent tracks in SiC under irradiation conditions with this electronic energy loss values. According to Sorieul et al. [16] the energy required has to be greater than 35 keV nm^{-1} .

The maximum dpa is found at $13.00 \mu\text{m}$ and the projected range was $13.02 \mu\text{m}$. The maximum dpa is less than the 0.3 dpa required for the armophizition of SiC [17]. For our samples, the epitaxial layer had a thickness of $6.0 \mu\text{m}$ which is less than the projected range. This shows that the Xe ions penetrated the epitaxial layer and were concentrated in the bulk layer. The layer therefore experienced mainly electron energy loss and only point defects were anticipated [16,18].

3.2. Raman spectroscopy

Raman spectroscopy was used to probe information about disorder,

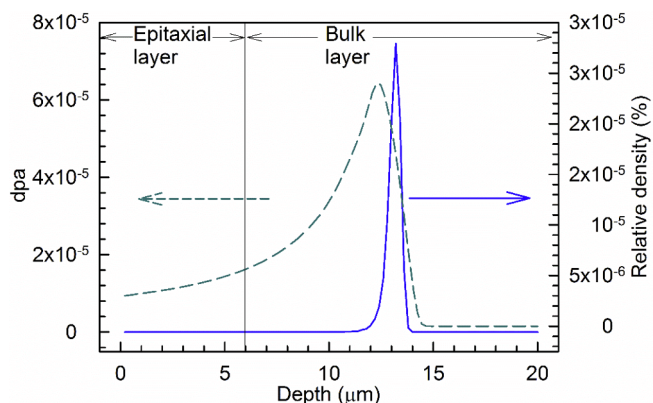


Fig. 1. Relative Xe density (%) and displacement per atom (dpa) as a function of depth obtained from SRIM simulations on 4H-SiC at a fluence of $5 \times 10^{11} \text{ cm}^{-2}$.

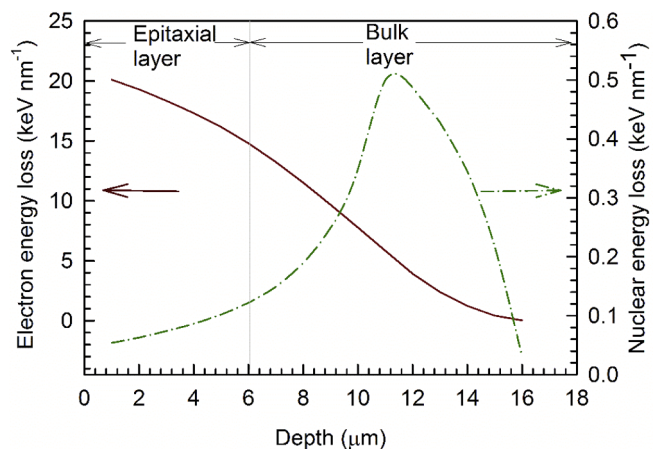


Fig. 2. Predicted electron and nuclear energy loss with depth.

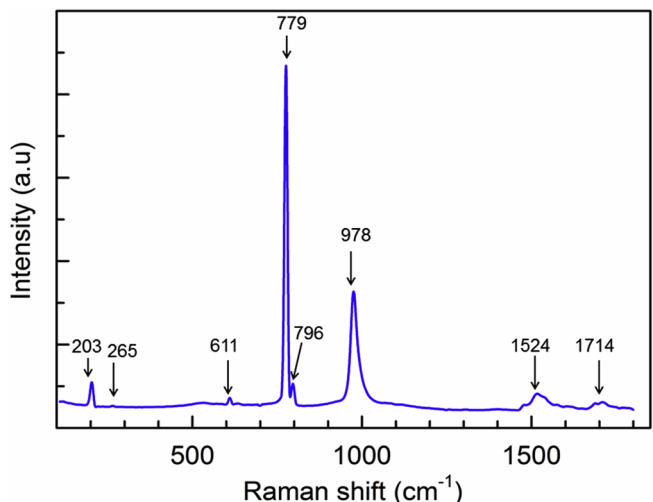


Fig. 3. Raman spectrum of pristine 4H-SiC.

stress and doping rate. It is a very valuable technique because it is a non-contact method [19]. Fig. 3 shows the Raman spectrum of pristine 4H-SiC samples in the $100\text{--}1800 \text{ cm}^{-1}$ range. 4H-SiC has a c -axis normal to the Si-C double atomic layers [20]. Transverse phonon coupling modes are perpendicular to the c -axis and the axial or longitudinal phonon coupling modes are parallel to the c -axis [19]. The spectrum shows peaks at $203, 265 \text{ cm}^{-1}$ corresponding to transverse acoustic

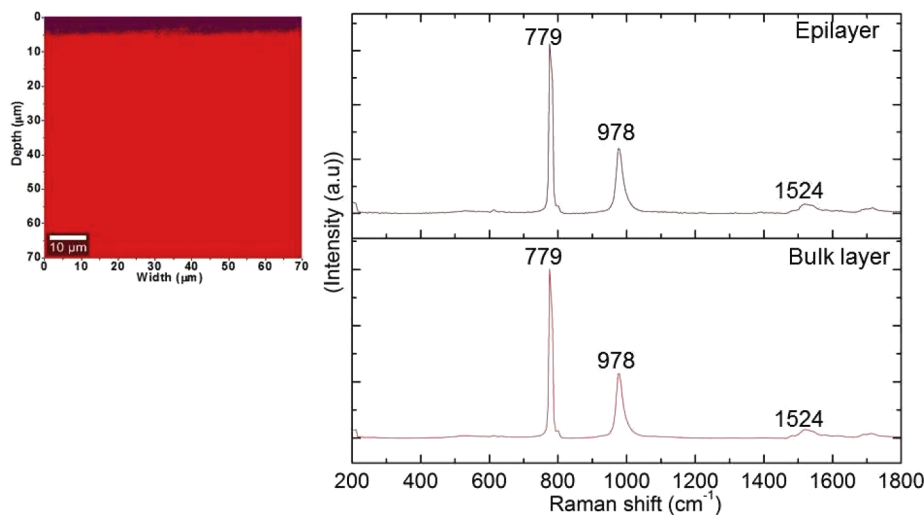


Fig. 4. (top left) Depth profile of as grown 4H-SiC obtained from cluster distributions showing an epitaxial layer (Brick red) and a bulk layer (bright red). The graphs show the cluster average Raman spectra which constitute the depth profile. (For interpretation of the references to colour in this figure legend, the reader is referred to the web version of this article.)

(TA) modes, and at 611 cm^{-1} peak which is a longitudinal acoustic (LA) mode [9]. The optical transverse (TO) and longitudinal (LO) peaks are observed at ($779, 796\text{ cm}^{-1}$), and 978 cm^{-1} , respectively. The LO at 978 cm^{-1} has been associated with free carrier (N-doping) interactions [21]. The material used had a relatively moderate doping which explains why the peak is less intense. In addition low intensity broad peaks at 1524 cm^{-1} and 1714 cm^{-1} are also observed on the spectrum corresponding to the optical branches. At around 500 cm^{-1} , a pedestal is observed, which according to Burton et al. is a feature of Raman scattering not luminescence since its spectral location is not changed at different laser wavelengths [19]. The peaks have been associated with vibrations of Si-Si, C-Si and C-C bonds.

3.3. Confocal Raman spectroscopy

Fig. 4 shows a depth profile and the associated cluster spectra of each layer of the wafer. An average cluster spectrum is generated by grouping data sets according to their similarities producing profiles showing areas where the data belongs [22]. The top layer (brick red) is approximately $6\text{ }\mu\text{m}$ thick. This is consistent with the thickness of the epitaxial layer as specified by the suppliers. The epitaxial layer is $6.0\text{ }\mu\text{m}$ (brick red) and the bright layer represents the bulk. The average cluster spectra shown in Fig. 4 are therefore a representation of the wafer structure with the spectrum for the epitaxial layer in brick red and the one for the bulk material in red. Table 1 lists the observed peaks. When compared, the LO peak at 779 cm^{-1} is slightly more intense on the epitaxial layer than in the bulk layer. However, peak intensity ratios $I_{978}:I_{779}$ are constant at 0.38 for both layers. This shows that difference in N-dopant concentration between the layers has an overall effect on the material not on individual vibrational modes.

Fig. 5 depicts the depth profile of the wafer (represented in Fig. 4) after 167 MeV Xe irradiation and the associated cluster spectra. Three layers are observed with a top thicker layer (blue) than in as grown samples, a medium layer (green) and the bulk layer (bright red). The top layer has a thickness of approximately $13\text{ }\mu\text{m}$. This value is consistent with the maximum dpa predicted from SRIM simulations. We

therefore speculate that the blue layer represents an average of part of the wafer with maximum damage induced by the incident radiation. The second layer (green) layer is not uniform which we speculate to be due to uneven damage resulting from a smaller population of the Xe ions which have maximum penetration depth as we move deeper into the bulk layer

The highest background is observed on the blue spectrum with a peak like structure at 883 cm^{-1} . Increase in background is disorder related. This shows that the top layer of the irradiated wafer had a relatively large amount of induced defects. The second layer (green) does not have a uniform spectral distribution on the depth profile; a clear boundary is not observed between the red and the green layer on the depth profile and disorder is observed on Fig. 5 at a depth up to twice the projected range. This uneven damage, according to Malherbe [23], can be attributed to a small population of displaced atoms recoiling through the lattice to produce other displacements resulting in a cascade effect and extended damage micro-regions. A similar result has also been observed by Hlatshwayo et al. [24] after irradiating SiC with slow moving 167 MeV Xe ions. The SRIM projected range was 160 nm but damage was observed at 190 nm . The observed peaks are listed in Table 2. The red layer represents the bulk of the wafer which was not penetrated by the incident irradiation.

A peak shift was observed on the longitudinal optical peak at 965 cm^{-1} on the different layers. Peak shifts have been associated with compressive stress in the c-plane due to lattice mismatch between layers. Jiang et al. [6] have shown that stress results from interstitial type defects or clusters formed by irradiation. Raman intensities of the irradiated samples are lower than those of the pristine samples Fig. 3. The peak intensity ratios $I_{978}:I_{779}$ were 0.52, 0.75 and 1.08 for the three layers respectively starting from the top. This can be explained as due to carrier removal, a phenomenon which occurs due to irradiation induced defects capturing carriers resulting in a reduced intensity of the N-dopant related 978 cm^{-1} . There is also a broadening of peaks as observed in the comparison of FWHM on Tables 1 and 2. The bulk layer is less intense on the bulk layer of irradiated samples because the irradiation damage increases optical absorption centres which reduces the Raman signal as it passes through the top layers.

When exposed to incident Xe radiation, ion solid interactions result in point defect generation that leads to lattice distortions due to electronic energy loss. Two well accepted models for the aftermath of the interactions are the thermal spike model and the coulomb explosion model [25,26]. Later on, ballistic processes in the nuclear energy loss regime, result in damage cascades with vacancies trapping gas particles and creation of interstitial defects [6]. The Raman spectra confirmed modifications to the crystal structure consistent with degradation

Table 1
Frequency and assignment of peaks for as grown epitaxial 4H-SiC.

Layer	Frequency (cm^{-1})	Mode	FWHM	Reference
Epitaxial	778	TO	11.3	[9]
Epitaxial	978	LO	22.3	[19]
Bulk	779	TO	10.2	[21]
Bulk	978	LO	21.4	[19]

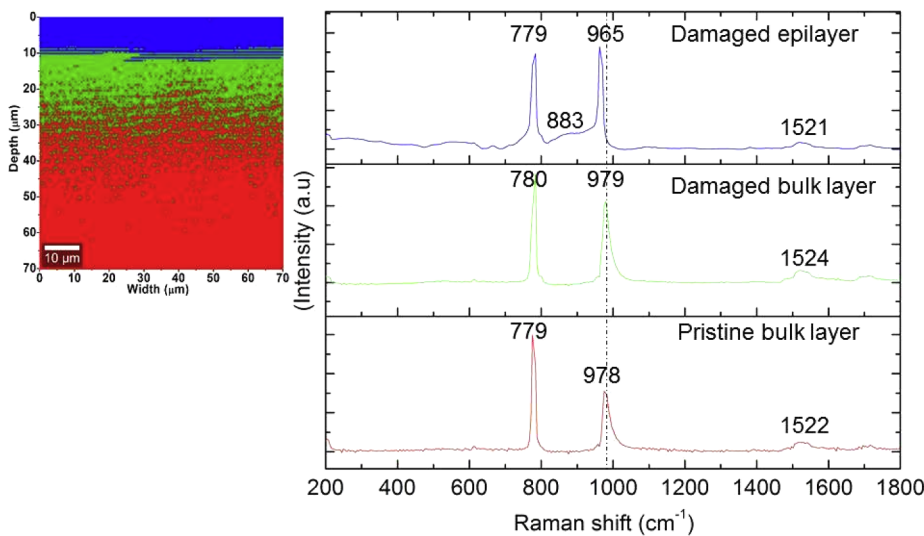


Fig. 5. (top left) Depth profile of 167 MeV Xe irradiated 4H-SiC obtained from cluster distributions showing a damaged epitaxial layer (blue), a damaged bulk layer (green) bulk layer (red). The graphs show the cluster average Raman spectra which constitute the depth profile. (For interpretation of the references to colour in this figure legend, the reader is referred to the web version of this article.)

Table 2

Frequency in cm and assignment for peaks for 167 MeV Xe irradiated epitaxial 4H-SiC.

Layer	Frequency (cm ⁻¹)	Mode	FWHM	Reference
Damaged epitaxial	779	TO	14.5	[9]
Damaged epitaxial	965	LO	13.2	[19]
Damaged Bulk	780	TO	13.5	[21]
Damaged Bulk	979	LO	21.7	[19]
Pristine Bulk	779	TO	10.2	[21]
Pristine Bulk	978	LO	21.3	[19]

without armophization. The projected dpa level is so low that no severe disorder can be created. A relatively low fluence was used, therefore, the bond structure and lattice order is to a greater extent preserved and the electronic structure has minor perturbations [16].

The decrease in Raman intensity after irradiation is attributed to decrease in Raman polarizability because of the breaking of bonds and changes in atomic force displacements. Loss in Raman signal has been correlated to optical absorption by point defects created in the bandgap [16]. Depth profiles from irradiated samples were consistent with SRIM simulation results. Maximum density of Xe ions is around 13 μm in where nuclear energy loss is at its maximum (Fig. 2). This shows that confocal Raman depth profiles can give results comparable to those obtained by binary collision approximations regarding the distribution of defects in the lattice structure.

3.4. Atomic force microscopy

Fig. 6 depicts the morphology of 4H-SiC obtained in Scanasyst mode. Fig. 6 a) shows pristine 4H-SiC and Fig. 6b shows irradiated 4H-SiC. It is clear that the irradiated material has elongated protrusions on the surface in the direction of the incident irradiation. Compositional analysis on these structures using energy dispersive X-ray analysis (EDS) showed that they were purely Si and C and were not emanating from any contamination of the samples. Ochedowski et al. [27] irradiated 6H-SiC with 81 MeV Ta²⁴⁺ and 117 MeV Pb³¹⁺ at angles of incidence varying from 0.6° to 1.1°. They observed narrow graphitic grooves and speculated that they emanated from the sublimation of silicon atoms in the SiC matrix by incident ions. From the AFM micrographs the areal density of the protrusions with ion dose is not direct. This discrepancy and the origin of these protrusions is still under investigation.

3.5. Deep level transient spectroscopy

Fig. 7 shows two DLTS spectra obtained using the 50 s⁻¹ rate windows. Curve (a) is the control spectrum obtained from un-irradiated samples and curve (b) is from samples irradiated with a fluence of $5 \times 10^{12} \text{ cm}^{-2}$ Xe⁺²⁶ ions. In the nomenclature used here E represents the electron trap and the number for example 0.10 represents activation enthalpy below the bandgap. The defects on curve (a) are the E_{0.09}, E_{0.12}, E_{0.15} and E_{0.65}. From curve (b) we notice that Xe irradiation introduced two electron traps E_{0.40} and E_{0.71} in addition to the native ones. A similar observation was made by Kalinina et al. in Kr irradiated 4H-SiC [11]. The defect signatures (activation energy E_a and capture cross section (σ_c) was determined from the slope and the apparent capture cross section was deduced from the slopes of Arrhenius plots in Fig. 8 using Eq. (1). The electronic properties and of all defects observed in this study are listed in Table 3.

The E_{0.09} has been attributed to a nitrogen impurity that occupy a cubic site. The E_{0.12} and E_{0.15} have been attributed to titanium impurities whereas the E_{0.65} has been identified as the Z₁ defect [28]. The Z₁ defect is a very important defect in 4H-SiC. It exhibits negative U behaviour.

The defect with energy approximately E_{0.71} was also detected by Doyle et al. after 20 MeV electron irradiation. Using secondary ion mass spectroscopy, they suggested that the defect is of intrinsic nature and is not related to any transition metals [29]. Storasta et al. used DLTS on low energy electron irradiated 4H-SiC and attributed the E_{0.71} and E_{0.41} to different charge states of the same defect [30]. Hemmingson et al. showed that the Z₁/Z₂ complex defect has negative U behaviour with an acceptor charge state of the Z₂ at 0.71 eV below the conduction band minima and a donor level of the Z₁ at approximately 0.41 eV [31]. This negative U system has also been observed using electronic paramagnetic resonance and DLTS [32]. Eberlein et al. modelled this system of defects using spin polarised density functional theory, as a stable π bonded di-carbon interstitial complex next to a nitrogen atom [33]. The introduction of the E_{0.71} and the E_{0.40} defects therefore is consistent with the introduction of the acceptor level of the Z₂ defect and the donor level of the Z₁ defect. These defects have also been observed in n-4H-SiC after irradiation by radionuclides and after metallization processes in 4H-SiC [2,34]. As a result none of the electrically active defect states can be directly attributed to Xe reactions with silicon carbide. The induced electrically active defects are both point defects and complexes.

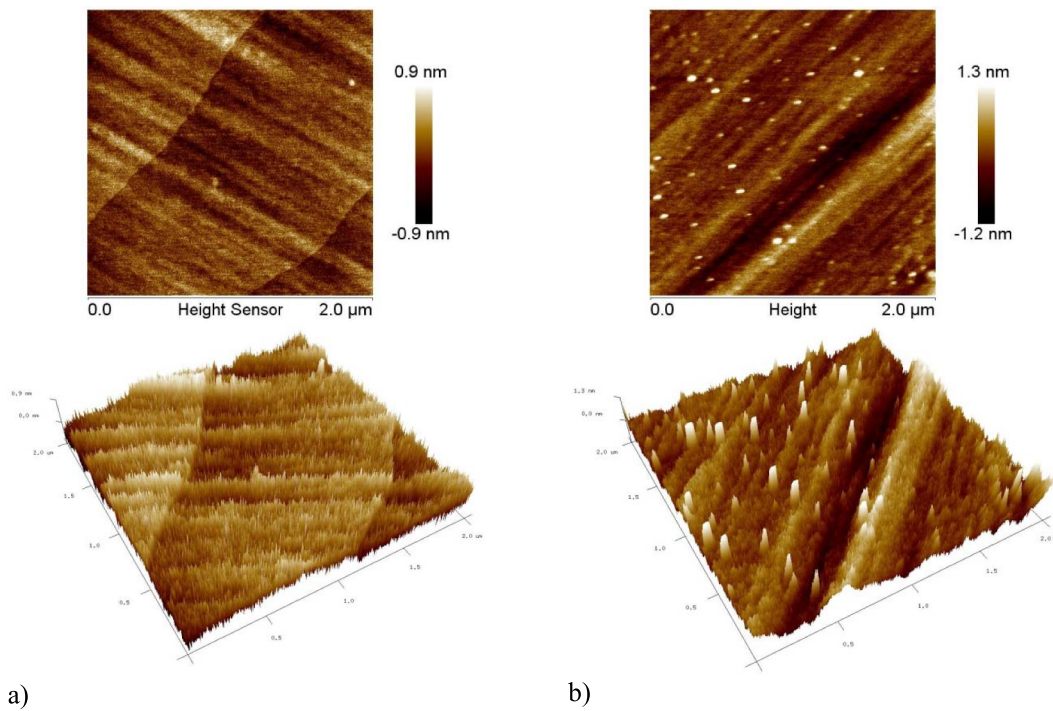


Fig. 6. $1.2 \mu\text{m} \times 2 \mu\text{m}$ AFM 2D and 3D images for a) pristine and b) 167 MeV Xe irradiated 4H-SiC.

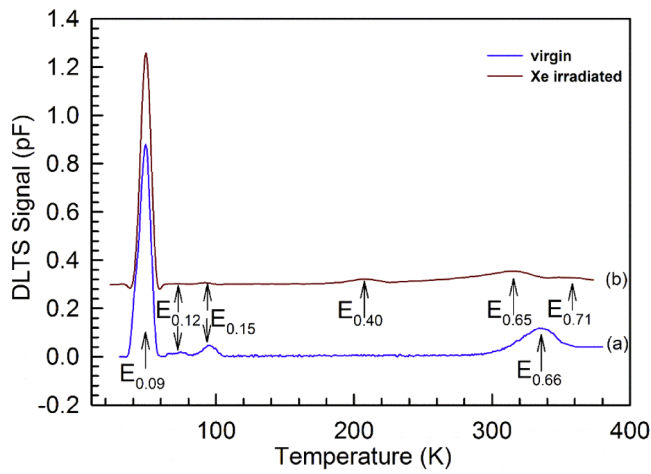


Fig. 7. DLTS spectra of un-irradiated and Xe irradiated 4H-SiC. The spectra were recorded using a reverse bias of -5 V , filing pulse of 1 V , filing pulse width of 2 ms and emission rate window of 50 s^{-1} .

4. Conclusions

n-type 4H-SiC was irradiated with swift heavy Xe^{+26} ions at room temperature. Structural disorder and point defects induced by the irradiation were investigated. From the Raman spectroscopy it was observed that the damage was moderate and the lattice structure was conserved. This was despite a SRIM maximum depth of $13.02 \mu\text{m}$. Confocal Raman spectroscopy depth profiles showed that there was a high density of disorder in the electron energy loss regime. Atomic force microscopy (AFM) showed that the incident radiation resulted in the formation of elongated protrusions. Ni Schottky barrier diodes were fabricated on swift heavy ion irradiated epitaxial layers and characterised with DLTS. The DLTS results are consistent with the swift heavy ions inducing the $E_{0.71}$ donor level of the Z_1 center and the $E_{0.40}$ acceptor level of the Z_2 center. From the confocal Raman spectroscopy results and the DLTS we can deduce that when n-type 4H-SiC is

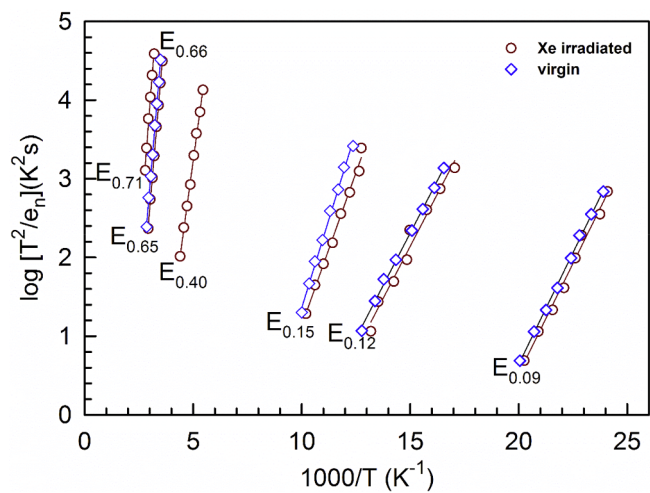


Fig. 8. Arrhenius plot of defects in resistively evaporated Ni/4H-SiC Schottky barrier diodes. One sample was subjected to Xe irradiation while the other was a control sample.

Table 3

Electronic properties of defects in as deposited Ni/n-4H-SiC Schottky barrier diodes made on Xe irradiated epitaxial layers and (un-irradiated) control samples.

Defect label	Energy (meV)	$\sigma_n (\text{cm}^{-2})$
$E_{0.09}$	89	1.3×10^{-11}
$E_{0.12}$	120	1.7×10^{-14}
$E_{0.15}$	151	1.3×10^{-16}
$E_{0.40}$	399	2.0×10^{-15}
$E_{0.65}$	646	4.0×10^{-15}
$E_{0.66}$	664	6.0×10^{-15}
$E_{0.71}$	708	1.7×10^{-15}

irradiated with swift heavy Xe^{+26} ions, density of the induced electrically active defects is higher in the region where electron energy loss is dominant.

References

- [1] B.L. Oksengendler, S.E. Maksimov, N.N. Turaeva, F.G. Djurabekova, Synergetic theory of catastrophic failures in the problem of radiation stability of solid-state electronics materials, *Nucl. Instrum. Meth. Phys. Res. Sect. B* 326 (2014) 45–47.
- [2] A.T. Paratzah, F.D. Auret, M.J. Legodi, E. Omotoso, M. Diale, Electrical characterization of 5.4 MeV alpha-particle irradiated 4H-SiC with low doping density, *Nucl. Instrum. Meth. Phys. Res. Sect. B* 358 (2015) 112–116.
- [3] W.J. Weber, L.M. Wang, N. Yu, N.J. Hess, Structure and properties of ion-beam-modified (6H) silicon carbide, *Mater. Sci. Eng. A* 253 (1998) 62–70.
- [4] A. Heft, E. Wendler, T. Bachmann, E. Glaser, W. Wesch, Defect production and annealing in ion implanted silicon carbide, *Mater. Sci. Eng. B* 29 (1995) 142–146.
- [5] L.L. Snead, J.C. Hay, Neutron irradiation induced amorphization of silicon carbide, *J. Nucl. Mater.* 273 (1999) 213–220.
- [6] C. Jiang, J. Nicolai, A. Declémé, E. Gilabert, M.F. Beaufort, J.F. Barbot, Implantation damage in heavy gas implanted 4H-SiC, *Nucl. Instrum. Meth. Phys. Res. Sect. B: Beam Interact. Mater. At.* 374 (2016) 71–75.
- [7] C. Claeys, E. Simoen, *Radiation Effects in Advanced Semiconductor Materials and Devices*, Springer Science & Business Media, 2013.
- [8] S.M. Tunhuma, F.D. Auret, J.M. Nel, E. Omotoso, H.T. Danga, E. Igumbor, M. Diale, Electrical characterization of defects induced by electron beam exposure in low doped n-GaAs, *Nucl. Instrum. Methods Phys. Res., Sect. B* 409 (2017) 36–40.
- [9] S. Sorieul, J.M. Costantini, L. Gosmain, L. Thomé, J.J. Grob, Raman spectroscopy study of heavy-ion-irradiated α -SiC, *J. Phys.: Condens. Matter* 18 (2006) 5235.
- [10] E.V. Kalinina, A.A. Lebedev, E. Bogdanova, B. Berenquier, L. Ottaviani, G.N. Violina, V.A. Skuratov, Irradiation of 4H-SiC UV detectors with heavy ions, *Semiconductors* 49 (2015) 540–546.
- [11] E. Kalinina, G. Onushkin, D. Davidov, A. Hallen, A. Konstantinov, V. Skuratov, J. Stano, Electrical study of 4H-SiC irradiated with swift heavy ions, *Semiconducting and Insulating Materials*, 2002. SIMC-XII-2002, in: 12th International Conference on, IEEE, pp. 106–109.
- [12] A. Bouille, A. Debelle, Statistical nature of atomic disorder in irradiated crystals, *Phys. Rev. Lett.* 116 (2016) 245501.
- [13] J.B. Wallace, L.B.B. Aji, T.T. Li, L. Shao, S.O. Kucheyev, Damage buildup in Ar-ion-irradiated 3C-SiC at elevated temperatures, *J. Appl. Phys.* 118 (2015) 105705.
- [14] S.M. Tunhuma, F.D. Auret, M.J. Legodi, M. Diale, The fine structure of electron irradiation induced EL2-like defects in n-GaAs, *J. Appl. Phys.* 119 (2016) 145705.
- [15] R.E. Stoller, M.B. Toloczkó, G.S. Was, A.G. Certain, S. Dwaraknath, F.A. Garner, On the use of SRIM for computing radiation damage exposure, *Nucl. Instrum. Meth. Phys. Res. Sect. B* 310 (2013) 75–80.
- [16] S. Sorieul, X. Kerbirou, J.M. Costantini, L. Gosmain, G. Calas, C. Trautmann, Optical spectroscopy study of damage induced in 4H-SiC by swift heavy ion irradiation, *J. Phys.: Condens. Matter* 24 (2012) 125801.
- [17] J.H. O'Connell, V.A. Skuratov, A.S. Sohatsky, J.H. Neethling, 1.2 MeV/amu Xe ion induced damage recovery in SiC, *Nucl. Instrum. Meth. Phys. Res. Sect. B* 326 (2014) 337–340.
- [18] M. Backman, M. Toulemonde, O.H. Pakarinen, N. Juslin, F. Djurabekova, K. Nordlund, A. Debelle, W.J. Weber, Molecular dynamics simulations of swift heavy ion induced defect recovery in SiC, *Comput. Mater. Sci.* 67 (2013) 261–265.
- [19] J.C. Burton, L. Sun, M. Pophristic, S.J. Lukacs, F.H. Long, Z.C. Feng, I.T. Ferguson, Spatial characterization of doped SiC wafers by Raman spectroscopy, *J. Appl. Phys.* 84 (1998) 6268–6273.
- [20] J. Fan, P.K. Chu, General properties of bulk SiC, *Silicon Carbide Nanostructures*, Springer, 2014, pp. 7–114.
- [21] S.-I. Nakashima, H. Harima, Raman investigation of SiC polytypes, *Phys. Status Solidi A* 162 (1997) 39–64.
- [22] J. Toporski, T. Dieing, O. Hollricher, *Confocal Raman Microscopy*, Springer International Publishing, 2018.
- [23] J.B. Malherbe, Diffusion of fission products and radiation damage in SiC, *J. Phys. D Appl. Phys.* 46 (2013) 473001.
- [24] T. Hlatshwayo, J. O'Connell, V. Skuratov, E. Wendler, E. Njoroge, M. Mlambo, J. Malherbe, Comparative study of the effect of swift heavy ion irradiation at 500°C and annealing at 500°C on implanted silicon carbide, *RSC Adv.* 6 (2016) 68593–68598.
- [25] A. Debelle, M. Backman, L. Thomé, W.J. Weber, M. Toulemonde, S. Mylonas, A. Boulle, O.H. Pakarinen, N. Juslin, F. Djurabekova, K. Nordlund, F. Garrido, D. Chaussende, Combined experimental and computational study of the recrystallization process induced by electronic interactions of swift heavy ions with silicon carbide crystals, *Phys. Rev. B* 86 (2012) 100102.
- [26] Z. Li, Q. Wang, Molecular dynamics simulation of Coulomb explosion in SiC, Progress report on nuclear science and technology in China (Vol. 3), in: Proceedings of academic annual meeting of China Nuclear Society in 2013, No. 4-nuclear material sub-volume, 2014.
- [27] O. Ochedowski, O. Osmani, M. Schade, B.K. Bussmann, B. Band'Etat, H. Lebuis, M. Schleberger, Graphitic nanostripes in silicon carbide surfaces created by swift heavy ion irradiation, *Nat. Commun.* 5 (2014) 3913.
- [28] A.T. Paratzah, E. Omotoso, M.J. Legodi, F.D. Auret, W.E. Meyer, M. Diale, Electrical characterization of high energy electron irradiated Ni/4H-SiC Schottky barrier diodes, *J. Electron. Mater.* (2016) 1–6.
- [29] J.P. Doyle, M.K. Linnarsson, P. Pellegrino, N. Keskitalo, B.G. Svensson, A. Schöner, N. Nordell, J.L. Lindström, Electrically active point defects in n-type 4H-SiC, *J. Appl. Phys.* 84 (1998) 1354–1357.
- [30] L. Storasta, J.P. Bergman, E. Janzén, A. Henry, J. Lu, Deep levels created by low energy electron irradiation in 4H-SiC, *J. Appl. Phys.* 96 (2004) 4909–4915.
- [31] C.G. Hemmingsson, N.T. Son, A. Ellison, J. Zhang, E. Janzén, Negative-U centers in 4H silicon carbide, *Physical Review B* 58 (1998) R10119–R10122.
- [32] N.T. Son, X.T. Trinh, L. Lovlie, B. Svensson, K. Kawahara, J. Suda, T. Kimoto, T. Umeda, J. Isoya, T. Makino, Negative-U system of carbon vacancy in 4 H-SiC, *Phys. Rev. Lett.* 109 (2012) 187603.
- [33] T.A.G. Eberlein, R. Jones, P.R. Briddon, Z_1/Z_2 defects in 4H-SiC, *Phys. Rev. Lett.* 90 (2003) 225502.
- [34] E. Omotoso, W.E. Meyer, S.M.M. Coelho, M. Diale, P.N.M. Ngoepe, F.D. Auret, Electrical characterization of defects introduced during electron beam deposition of W Schottky contacts on n-type 4H-SiC, *Mater. Sci. Semicond. Process.* 51 (2016) 20–24.